ELSEVIER

NeuroImage

www.elsevier.com/locate/ynimg
NeuroImage 37 (2007) 177–188

Reducing the unwanted draining vein BOLD contribution in fMRI with statistical post-processing methods

Andrew S. Nencka and Daniel B. Rowe*

Department of Biophysics, Medical College of Wisconsin, 8701 Watertown Plank Road, Milwaukee, WI 53226, USA

Received 6 October 2006; revised 15 March 2007; accepted 19 March 2007
Available online 3 May 2007

Recent BOLD fMRI data analysis methods show promise in reducing contributions from draining veins. The phase regressor method developed by [Menon, R.S., 2002. Post-acquisition suppression of large-vessel BOLD signals in high-resolution fMRI. Magn. Reson. Med., 47, 1–9] creates phase and magnitude images, regresses magnitude as a function of phase, and subtracts phase-estimated magnitudes from the observed magnitudes. The corrected magnitude images are used to compute cortical activations. The complex constant phase method, developed by [Rowe, D.B., Logan, B.R., 2004. A complex way to compute fMRI activation. NeuroImage, 23, 1078–1092], uses complex-valued reconstructed images and a nonlinear regressor model to compute magnitude cortical activations assuming temporally constant phase. In both methods, the usage of the phase information is claimed to bias against voxels with task-related phase changes caused by some draining veins. The behavior of the statistical methods in data with several task-related magnitude and phase changes is compared. The power of the statistical methods for determining voxels with specific task-related magnitude and phase change combinations are determined in ideal simulated data. The phase regressor and complex constant phase activation determination techniques are examined to characterize the responses of the models to select task-related phase and magnitude change combinations in representative simulated time series. Possible draining veins in human preliminary data are discussed and analyzed with the models and the current challenges which prevent these methods from being reliably implemented are discussed.
© 2007 Elsevier Inc. All rights reserved.

Introduction

The measured signal in MRI can be encoded to represent the complex-valued Fourier transform (FT) of the object being imaged. The image is generally reconstructed by performing an inverse Fourier transform (IFT) on the collected data (Rowe et al., 2007b). The object is physical, and is thus real-valued. Therefore, under ideal conditions, the FT of the object would result in observed complex-valued data and the IFT of this data would result in the reconstruction of the unaltered, real-valued image of the object. However, small-scale inhomogeneities in the magnetic field and measurement noise lead to complications in this mathematical treatment of the data (Haacke et al., 1999). The reconstructed image is thus complex-valued, and can be visualized through a unique representation in real and imaginary images.

Functional MRI (fMRI) traditionally relies upon the statistical analysis of time series of magnitude-only images using blood oxygen level-dependent (BOLD) contrast to determine areas of cortical activation (Ogawa et al., 1993; Bandettini et al., 1993; Cox et al., 1995). Because popular methods of determining brain activation through fMRI only utilize magnitude images over the experimental time course, they discard information about small-scale magnetic field disturbances contained in the complex-valued data, or phase image time course (Rowe and Logan, 2004). This phase data is often corrupted by physiologic processes, slight subject motion and other noise (Pfeuffer et al., 2002). In spite of the noise in this data, some have proposed using the information in this data to improve the detection power of activation methods (Lai and Glover, 1997; Nan and Nowak, 1999). Others have directly used the phase information alone to detect activations (Rowe et al., 2007a). This phase data, related to local magnetic field changes, may hold a great deal of information about the source of the BOLD signal.

The BOLD signal arises from changes in blood oxygenation, and is thus sensitive to the capillaries where the oxygenation change occurs and downstream draining veins. With activation the concentration of oxyhemoglobin in the active capillaries and veins increases, effectively altering the blood's susceptibility. This leads to a change in the magnetic field within active vessels which correlates with the activity. Thus, the magnetization within these active vessels will acquire a different net phase with activation than with rest. If the active vessels within a voxel are large well-oriented draining veins which contribute strongly to the observed signal, they will contribute a task-related phase change (Menon, 2002). Smaller venules and capillaries located in the parenchymal tissue, which are more randomly oriented, more densely packed, and carry a smaller volume of blood, lead to random de-phasing without a preferential direction. Therefore, because of these randomly oriented phase alterations within a voxel in the parenchyma, the

* Corresponding author.
E-mail address: dbrowe@mcw.edu (D.B. Rowe).
Available online on ScienceDirect (www.sciencedirect.com).

1053-8119/$ - see front matter © 2007 Elsevier Inc. All rights reserved.
doi:10.1016/j.neuroimage.2007.03.075

signal will decay but will not exhibit a coherent phase change. The orientation of the vessels with respect to the magnetic field, and many other variables, will obviously affect the strength of the task-related phase change (TRPC), as it will be minimized, for instance, with the vein at the "magic angle". Thus voxels with TRPCs will most likely be contaminated by the macrovasculature while it is not certain that voxels without TRPCs are free from draining veins (Klassen and Menon, 2005).

Because it is believed that the most relevant cortical activations detected through BOLD contrast are those which are tied to the microvasculature where the blood oxygenation change occurs, many attempts have been made to reduce the contributions from the macrovasculature, or large draining veins, to the BOLD-computed cortical activations. In standard resolution fMRI, activations from draining veins are generally not of concern as such veins are co-localized in voxels with active parenchyma. Further downstream, the venous blood is diluted resulting in less signal change. It has been shown that with an active cortex area of 100 mm^2 such dilution is observable about 4 mm downstream from the active cortex, with only 1/4 of the oxygenation change of active cortex up to 25 mm away (Turner, 2002). In higher-resolution fMRI, however, this draining vein signal becomes more problematic. Draining vein contributions are less consistently co-localized in voxels with active parenchyma and they may be several voxels away from the active cortex. Furthermore, smaller voxel volume leads to attenuated partial volume effects and intra-voxel de-phasing, allowing draining veins to have a greater influence in the signal of downstream voxels. Thus, the de-localization of activations from draining veins becomes problematic when higher resolution fMRI is used.

It is the goal of this paper to explore two recently proposed post-processing methods which utilize the magnitude and phase components of the complex-valued signal to determine BOLD cortical activations. It has been suggested that the complex phase regressor method localizes computed activations to the parenchyma by reducing draining vein contributions (Menon, 2002). Likewise, Rowe and Logan's method of magnitude activation in complex data assuming constant phase has been claimed to both localize activations to the parenchyma and reduce the draining vein component of activations (Rowe and Logan, 2004; Rowe, 2005a; Nencka and Rowe, 2005). In this study, we compare the ability of the two statistical techniques to bias against voxels which exhibit task-related phase changes under ideal simulated conditions. We also discuss the application of these techniques to preliminary experimental data and several confounding factors which must be resolved for such phase-based draining vein identification to be practically implemented.

Statistical methods

We first briefly outline the parameterization of the advanced statistical activation detection techniques and offer illustrative simulated voxel time series. Both the phase regressor and complex constant phase methods employ the use of general linear models. Simple general linear models are well developed in the literature. Further descriptions of the implementations of the phase regressor and complex constant phase models are given in Appendices A and B.

The phase regressor method (Menon, 2002) assumes normally distributed noise on the magnitude and phase data. The model also assumes that task-related magnitude changes associated with draining veins are linearly related to the task-related phase changes of those veins. Assuming errors in both variables, the magnitude values for a time series are regressed as a function of the corresponding phase values for a given voxel. Based upon each phase time point value, an estimated magnitude is determined using the computed regression. This phase-estimated magnitude is then subtracted from the observed magnitude to discount the phase associated magnitude component in a "phase-corrected" magnitude time series. The common magnitude-only general linear model is then used to analyze the corrected magnitude time series.

Examples of this method are illustrated through simulated voxel time series shown in Fig. 1. The simulated data were created using the complex-valued general linear model as described by Rowe (2005b):

$$Y_t = [(\beta_0 + \beta_1 t + \beta_2 x_{2t})\cos(\gamma_0 + \gamma_1 t + \gamma_2 x_{2t}) + \eta_{Rt}] + i[(\beta_0 + \beta_1 t + \beta_2 x_{2t})\sin(\gamma_0 + \gamma_1 t + \gamma_2 x_{2t}) + \eta_{It}]. \quad (2.1)$$

In all cases, no linear trend was modeled in phase, $\gamma_1 = 0$, and β_2, γ_2, and β_0 were set to determine the contrast-to-noise ratio (CNR $= \beta_2/\sigma$), task-related phase change (TRPC $= \gamma_2 * 180/\pi$), and signal-to-noise ratio (SNR $= \beta_0/\sigma$). In Figs. 1(A) and (D), the ideal magnitude time series (red), noise corrupted time series (green), phase corrected magnitude time series (blue) and phase regressor model fit (black) are shown. Figs. 1(B) and (E) depict the corresponding ideal and simulated phase time series. In Figs. 1(C) and (F), scatter plots of magnitude (vertical axis, in arbitrary units) and phase (horizontal axis, in degrees) are shown for time points during the active (star) and inactive (circle) periods. The regression for magnitude as a function of phase, accounting for errors in both variables, is shown by the solid black line.

The first row of Fig. 1 is for a time series with a very strong task-related magnitude changes (CNR = 1) and no task-related phase changes (TRPC = 0°), as would be expected in a voxel containing only parenchyma. It can be seen that the phase regressor method preserves the statistically significant block design in the corrected magnitude time series with reduced magnitude.

The second row of Fig. 1 depicts a time series with a moderate task-related magnitude change (CNR = 0.78) and moderate task-related phase change (TRPC = 2°), as could be expected in a voxel containing a draining vein. In this case, error in the fit of the magnitude as a function of the phase leads to a statistically insignificant overcorrection of the magnitude data in the phase corrected magnitude data. Thus, while the original magnitude-only time series exhibits a statistically significant block design, the corrected time series does not as the phase regressor method subtracts larger magnitude estimates from the observed magnitude time series during active blocks, reducing the statistical significance of the activation statistic.

The complex constant phase method (Rowe and Logan, 2004) aims to bias against time series which exhibit phase changes through an entirely different mechanism than the phase regressor model. The complex constant phase method models the entire complex-valued voxel time series in a general linear model. This statistical model assumes normally distributed noise on the complex-valued data and assumes that the phase is temporally fixed on a voxel-wise basis. Thus, the model simultaneously fits a block design to the magnitude data and a constant phase to the phase data. When a time series exhibits phase changes, the fit of the constant phase to the incorrectly modeled temporally varying phase leads to an increase in the variance of the residuals from the fit model. As it is shown in Appendix B, an increase in the variance

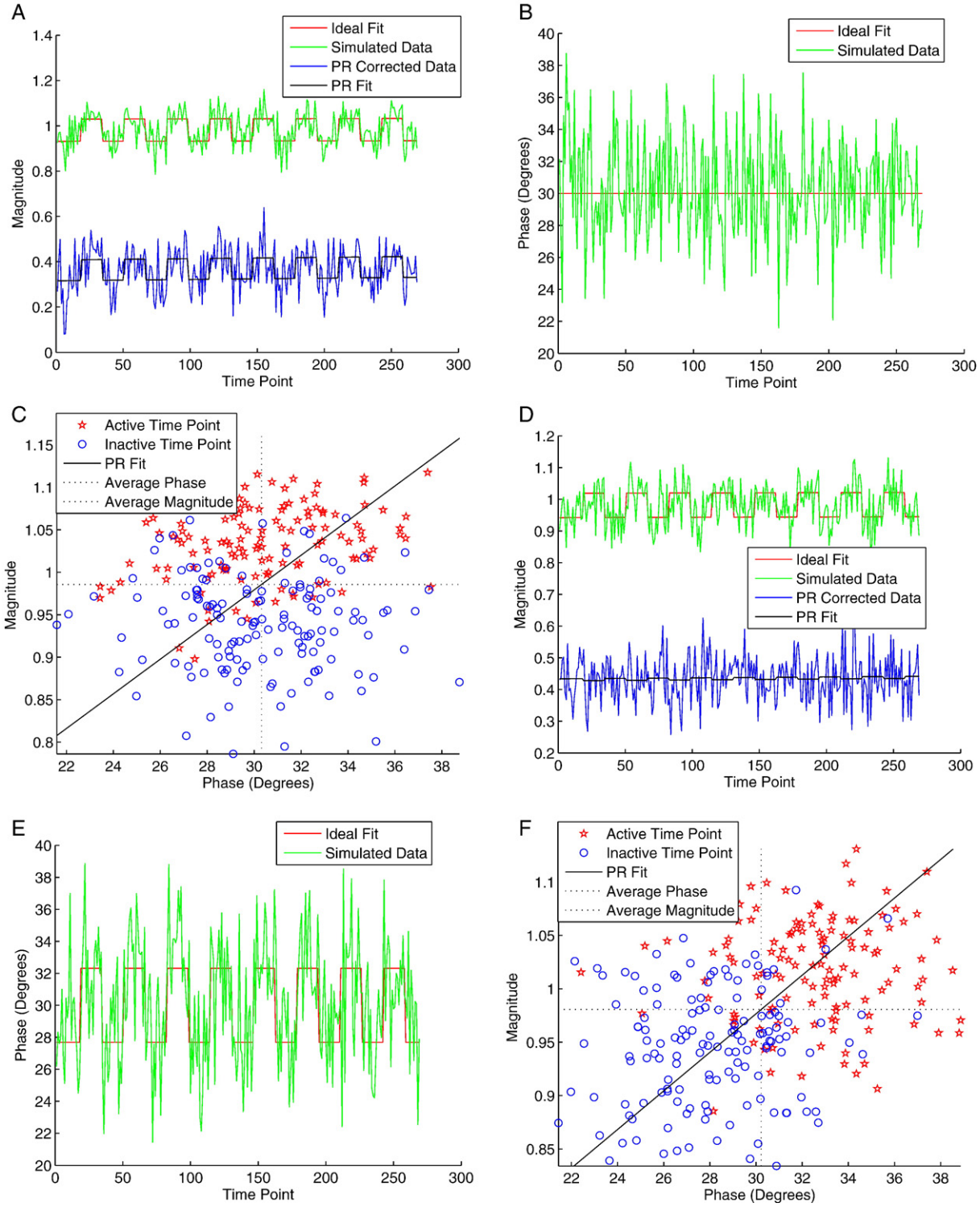

Fig. 1. Simulation Time Series for CNR = 1, TRPC = 0° (A, B, and C) and CNR = 0.78, TRPC = 2° (D, E, and F). Panels A and D illustrate the ideal magnitude time series (red), simulated magnitude time series (green), phase-corrected magnitude time series (blue) and fit phase regressor model (black). Panels B and E illustrate the ideal phase time series (red) and simulated phase time series (green). Panels C and F show scatter plots of the active (star) and inactive (circle) time points with phase (in degrees) on the horizontal axis and magnitude (in arbitrary units) on the vertical axis. The fit of magnitude as a function of phase for the phase regressor method is shown as a solid line and the mean phase angle and mean magnitude value are shown as dotted vertical and horizontal lines, respectively.

of the residuals from the fit model will lower the computed activation statistic. Thus, the bias against voxels with phase changes in the complex constant phase statistical method is achieved through the increase of the variance of the residuals from the model in voxels with phase changes. This is opposed to the empirical modeling of the magnitude-phase relationship deter-

mined in the phase-regressor model. Instead of modeling the draining vein response, the complex constant phase method relies upon a reduced statistical fit of the model in expected draining veins. This identification of veins based upon a reduced fit of the model, rather than directly modeling the venous response, can be a criticism of the complex constant phase statistical model.

Example time series for the constant phase method are shown in Fig. 2. The first row shows an active voxel with a strong magnitude change (CNR = 1) and no task-related phase change (TRPC = 0°). This data is the same as presented in Figs. 1(A), (B), and (C). The magnitude fit is in good correspondence to the data and is seen that the errors from the phase time series fit result only from the phase noise. The residual variance from this fit is identical to that of the magnitude-only fit. The second row includes a time series from a simulated voxel with a moderate magnitude change (CNR = 0.35) and large task-related phase change (TRPC = 4°). These parameters differ from those in Figs. 1(D), (E) and (F) as the models exhibit favorable vein-reducing characteristics with different CNR–TRPC combinations, as will be discussed in the next section. As in the previous case, the magnitude fit from the constant phase method is good, nearly corresponding to the ideal simulated data. However, the residuals of the phase model are inflated through the addition of the structured phase change in addition to the random phase noise. This leads to an increase in the variance of the fit model's residuals and a corresponding decrease in the associated activation statistic. Thus, the constant phase method biases against voxels with temporally non-constant phase, including voxels with task-related phase changes because of the reduced model fit to the data.

Computer simulation study

Methods

To examine the properties of these statistical activation detection methods under known conditions a simulation was performed in MATLAB (The Mathworks, Natick, MA, USA). In the simulation, time courses for each pixel of a 128 × 128 array were first created using the complex-valued general linear model defined in Eq. (2.1). In all cases, there was no linear trend in the phase ($\gamma_1 = 0$). All pixels were made active so that a non-zero contribution was made by the reference function to the magnitude and/or phase data ($\beta_2 = 0$ to σ and $\gamma_2 = 0$ to $5\pi/180$). The strengths

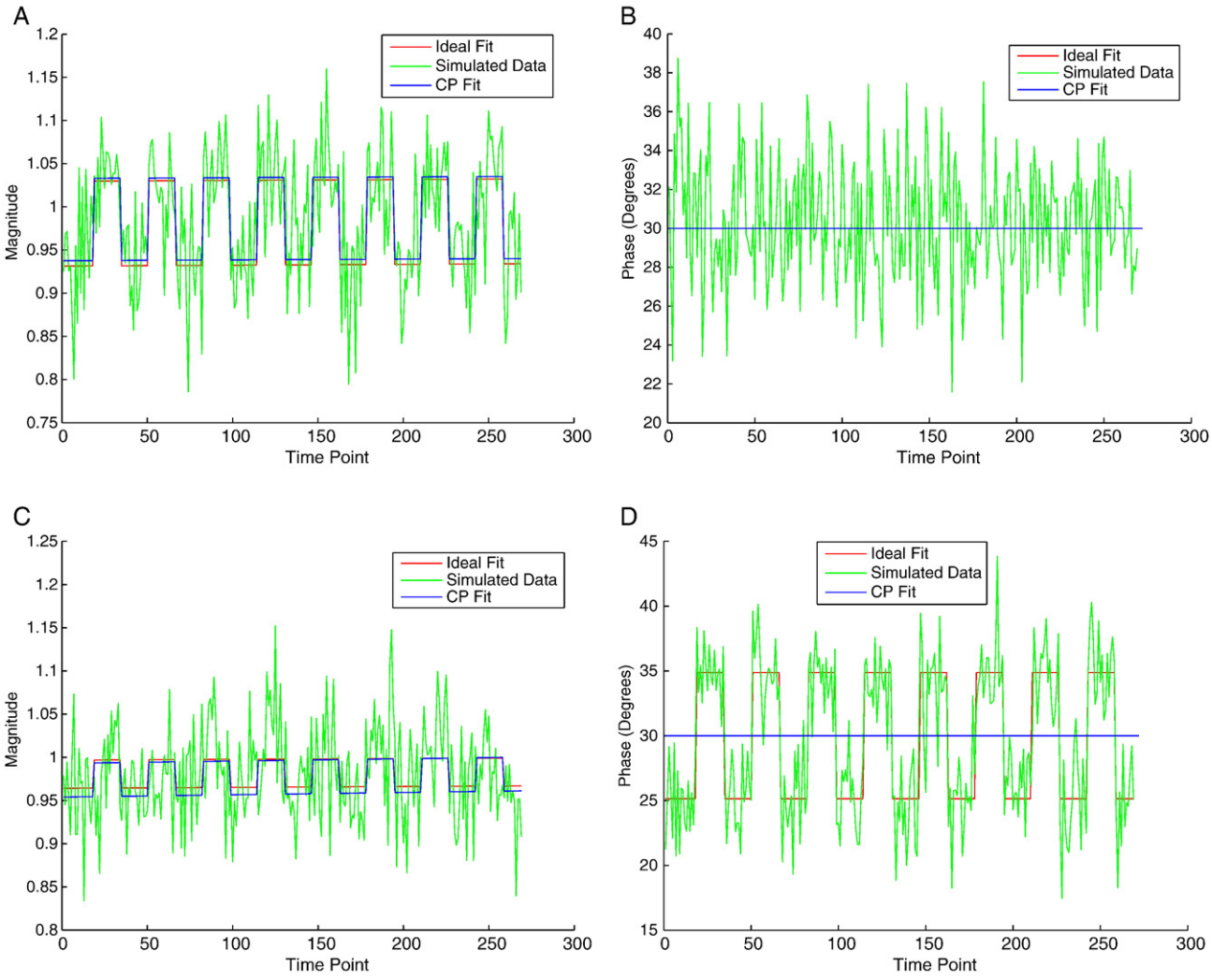

Fig. 2. Simulation time series for CNR = 1, TRPC = 0° (row 1) and CNR = 0.35, TRPC = 4° (row 2). Panels A and C illustrate the ideal magnitude time series (red), simulated magnitude time series (green), and constant phase fit (blue). Panels B and D illustrate the ideal phase time series (red), simulated phase time series (green), and constant phase regression fit (blue). The constant phase regression of the phase is coincident with the ideal phase time series in panel B.

of the magnitude contributions were determined by setting the temporal contrast-to-noise ratios (CNR = β_2/σ), and the strengths of the phase changes were determined by setting γ_2 values, and thus the number of degrees in the task-related phase changes (TRPCs). In all of the 128 × 128 pixels, the complex-valued simulated data was corrupted with randomly generated, normally distributed noise in the real and imaginary components with a temporal signal-to-noise ratio (SNR = β_0/σ) of 20. This temporal SNR approximately corresponds to the SNR measured in the human data presented later, as determined by the β_0 and σ terms in the magnitude-only general linear model regression. Each pixel of the 128 × 128 array was assigned a different CNR–TRPC combination, for a total of 16,384 separate combinations. One thousand iterations of computing activations on different generated data sets were performed to determine powers of the various method for declaring pixels active above an $\alpha = 0.05$ Bonferroni adjusted threshold in each iteration of this simulation (Logan and Rowe, 2004). The activation power for a method was defined to be the percentage of times in the one thousand data sets that a pixel was declared active by that method.

Results

The results of the simulation are shown in Fig. 3. The horizontal axis represents the CNR, as it changes from 0 on the left-hand side to 1 on the right-hand side in 128 equal steps, and the vertical axis represents the TRPC as it changes from 0° on the top to 5° on the bottom in 128 equal steps. Each subfigure depicts a surface indicating the power of each post-processing method for detecting activations with the varying CNR–TRPC combinations.

As shown in Figs. 3(A) and (B), both the magnitude-only and phase-only statistical methods are dependent upon only the CNR and the TRPC respectively. However, the complex constant phase and complex phase regressor analysis methods show obvious dependencies upon both the CNR and TRPC. As seen in Fig. 3(C), with small TRPCs, just like the magnitude-only method, the complex constant phase statistical method declares all voxels with significant CNRs active with high power. Such TRPC–CNR combinations are observed in parenchymal voxels. However, as TRPCs increase, this similarity between the magnitude-only and complex constant phase statistical methods diminishes, as also shown in an abstract by Nencka and Rowe (2006). When larger TRPCs are present in the time series, the constant phase method requires a higher CNR to declare voxels active. In the brain, such voxels with moderate CNRs and larger TRPCs include voxels which contain draining veins. Thus, this simulation suggests that the complex constant phase method may bias against such voxels which may contain draining veins. However, if a voxel contains both a large TRPC and CNR, the constant phase method declares the voxel active with the same power as the magnitude-only method. These TRPC–CNR combinations can result from large draining veins which exhibit extraordinarily large CNRs. In such cases, the constant phase method does not bias against the contaminated voxels. This suggests that the complex constant phase method may bias against some voxels with TRPCs while not removing all of them.

As shown in Figs. 3(D), (E) and (F), the phase regressor method yields more complicated results than the other methods which are more easily understood with the analysis of individual time series in Figs. 1 and 4. In the situations shown in Fig. 1, the phase regressor statistical method performs as expected when there are small TRPCs and large CNRs by biasing against time series with TRPCs. However, errors can be introduced into the analysis through errors in the regression of magnitude as a function of phase. Examples of such errors are shown in Fig. 4 as two simulated time series with identical parameters but different seed values for the random noise yield different phase regressor statistics. Slight errors in the estimation of the phase or magnitude variance needed for the fit assuming errors in both variables can lead to large variation in the fit. With small CNRs this leads to occasional over- and undercorrection of the magnitude signal. In Fig. 3(E), this is responsible for the band of moderate power with small CNRs. With larger CNRs, the errors in the fit from either overestimating the phase variance or underestimating the magnitude variance dominate as the magnitude time series are systematically overcorrected. In Fig. 3(F), this is responsible for the large region of determined negative correlation, although no negative correlation was simulated.

In the region where the phase regressor method performs as expected, it exhibits a bias against smaller TRPCs which is sharper than the complex constant phase method. Additionally the phase regressor method exhibits a bias against smaller CNRs with no TRPCs that the complex constant phase method does not exhibit.

This simulation on ideal data suggests that the complex constant phase method may exhibit a more conservative region of activations, possibly including some draining vein activations with large TRPCs. The phase regressor method may exhibit a more aggressive bias against draining veins under ideal conditions, but it also may include many false positives from slight errors in the regression of magnitude as a function of phase. Additionally, the constant phase statistical method retains the power of the magnitude-only method at low CNRs when no TRPCs are present while the phase regressor method requires a higher CNR to find activations.

Preliminary human experimental study

Methods

A preliminary human study was performed that consisted of a blocked design bilateral finger tapping experiment to yield activation in the primary motor cortex and an angiogram was obtained to identify large veins. The task consisted of resting 20 s, followed by 8 epochs of 16 s of tapping and 16 s of rest. Each subject ($N = 5$) performed the task while being imaged using a gradient recalled echo EPI pulse sequence. Scanning used a GE Signa LX 3 T scanner with a quadrature transmit/receive coil, where 10 axial slices of 96 × 96 were acquired in the motor cortex. Slices demonstrating activation in the primary motor cortex as well as superior slices containing draining large veins as identified in the angiogram were examined in this study. The scanning parameters for the EPI acquisitions included a minimum full *k*-space TE of 50 ms, TR of 2000 ms, flip angle of 80°, field of view of 19.2 cm, slice thickness of 2 mm, and 138 time points. This resulted in 2-mm isotropic voxels. Data was pre-processed to correct for minor *k*-space offsets in alternating lines caused by eddy currents. A time of flight spoiled gradient recalled echo pulse sequence was used to acquire an angiogram. Parameters for this sequence included an acquisition matrix of 256 × 256, TE of 5.1 ms, TR of 40 ms, flip angle of 40°, field of view of 24.0 cm, and slice thickness of 1.4 mm. This sequence saturates the

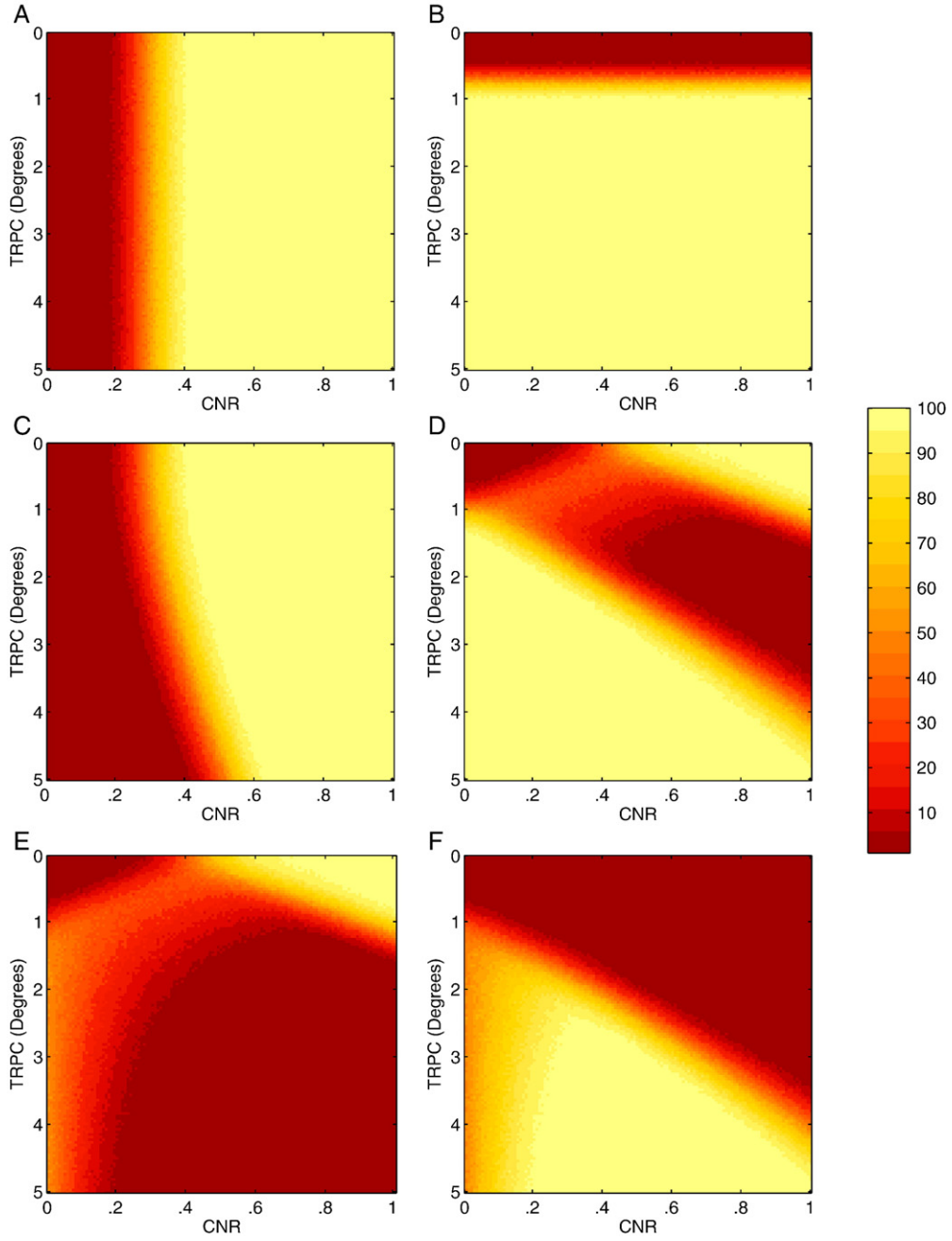

Fig. 3. Simulation z-statistic activation power surfaces. The magnitude-only (MO, A), phase-only (PO, B) and constant phase (CP, C) methods positive z-statistic power surfaces are identical to the shown unsigned surfaces. The MO and PO methods are dependent upon only CNR and task-related phase change (TRPC), respectively. The CP method biases against larger TRPCs. The phase regressor method (PR, D) includes positive and negative statistics. Positive z-statistic PR method E exhibits a sharp bias against TRPCs and fails if a voxel exhibits a small CNR. When large TRPCs are observed in voxels, the negative PR method F over-corrects for phase-related magnitude changes.

stationary tissue signal, allowing the unsaturated in-flowing blood to be imaged as a hyper-intense.

Algorithms developed in MATLAB (The Mathworks, Natick, MA, USA) were used to compute activations in the functional data. Before computing activations, an ideal 0/1 frequency filter (Gonzalez and Woods, 1992) was used to remove respiration and extremely low-frequency noise from signal drift in the voxel time courses (Smith et al., 1999). Also, the first three time points were removed from analysis to adjust for signal stabilization. Activation statistics were then computed using the magnitude-only statistical method unwrapped phase-only statistical method, phase regressor statistical method as described in Appendix A (Menon, 2002), and complex constant phase statistical method as described in Appendix B (Rowe and Logan, 2004). The resulting z-statistic activation maps were thresholded using a Bonferroni adjusted $\alpha = 0.05$ threshold on a per-slice basis (Logan and Rowe, 2004). No clustering techniques were considered to show the raw results of applying the statistical methods and because the methods were

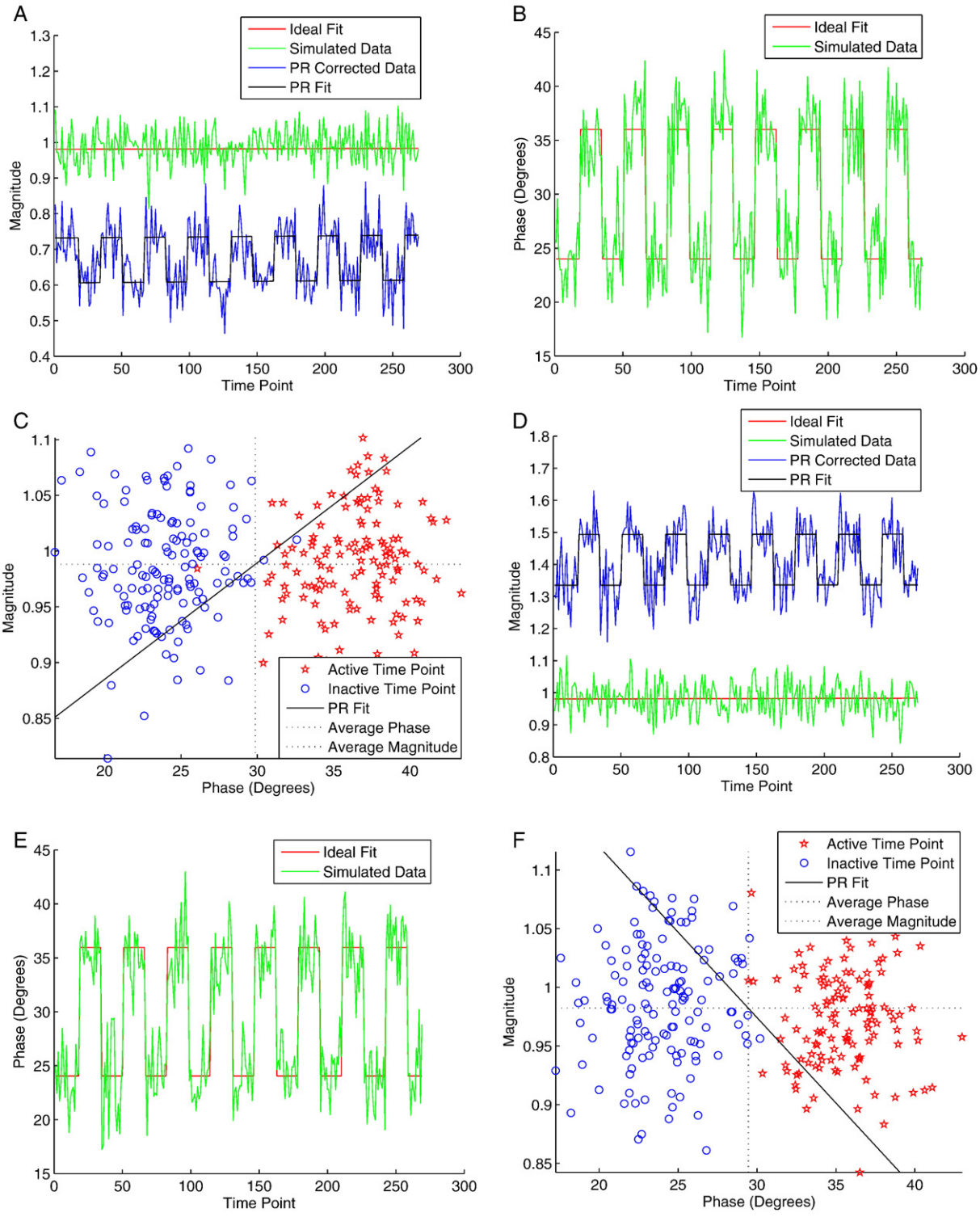

Fig. 4. Simulation time series for CNR = 0 and TRPC = 5°. Panels A, B, and C show a time series with the complex data corrupted by normal noise and panels D, E, and F show the same time series with the random noise generated by a different seed value. Panels A and D illustrate the ideal magnitude time series (red), simulated magnitude time series (green), phase-corrected magnitude time series (blue) and fit phase regressor model (black). Panels B and E illustrate the ideal phase time series (red) and simulated phase time series (green). Panels C and F show scatter plots of the active (star) and inactive (circle) time points with phase on the horizontal axis and magnitude on the vertical axis. The fit of magnitude as a function of phase for the phase regressor method is shown as a solid line and the mean phase angle and mean magnitude value are shown as dashed vertical and horizontal lines, respectively. The expected fit of the magnitude as a function of phase corresponds to the horizontal dotted line at the mean magnitude value.

originally presented assuming no spatial correlation in activations. Each thresholded activation map was overlaid on the first slice of the functional time series for anatomical reference. Additionally, the corresponding slices from the angiograms were examined to determine the localization of large draining veins.

In all subjects, eight axial slices were considered, with four through the active parenchyma and four through superior slices as pial veins draining the motor cortex run superiorly to the sagittal sinus. The slices with active parenchyma were chosen as the slices with the highest number of voxels with magnitude-only activation z-statistics above a slice-wise $\alpha = 0.05$ Bonferroni-adjusted threshold in the motor cortex. The superior slices with draining pial vein contributions were selected as slices at least 4 mm superior to the previously described slices and exhibited phase-only activations (Rowe et al., 2007a) along the cortical surface. These activations were near the central sulcus and coincided with the anatomical locations of pial veins in the angiogram. Furthermore, signal loss due to venous de-phasing was also observed in the regions of the expected draining veins. EPI slices were not registered to the corresponding angiogram slices because small-scale B-field inhomogeneities caused minor warping in the EPI images preventing accurate alignment with the small structures observed in the angiogram.

Preliminary results

Representative activation maps shown in Fig. 5. The anatomical underlays for these parenchymal and venous slices are shown in Figs. 6(A) and (C), respectively, with the angiograms shown in Figs. 6(B) and (D). Note that the activations in the parenchymal slice (Fig. 5(A)) do not correspond with hyper-intense signal in the angiograms while the activations in the venous slice (Fig. 5(E)) are well localized with the hyper-intense vascular signal in the venous slice. Furthermore, stronger negative activation statistics are found with the phase-only statistical method in the regions of the active veins in Fig. 5(F), while very few phase-only activations are found in the parenchymal slice in Fig. 5(B). Other less significant phase

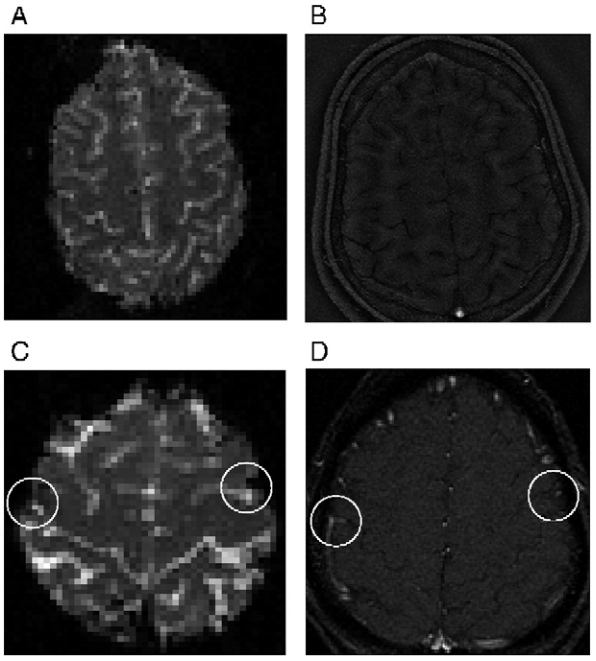

Fig. 6. The anatomical underlays for the representative parenchymal and venous slices shown in Fig. 5 are shown here in panels A and C. The corresponding time of flight angiograms from those slices are shown in panels B and D. The vasculature is imaged as hyper-intense in the angiogram, and it is apparent that the venous slice activations are co-localized with the imaged vasculature while the parenchymal slice activations are not. The locations of probable active veins are circled in panels C and D.

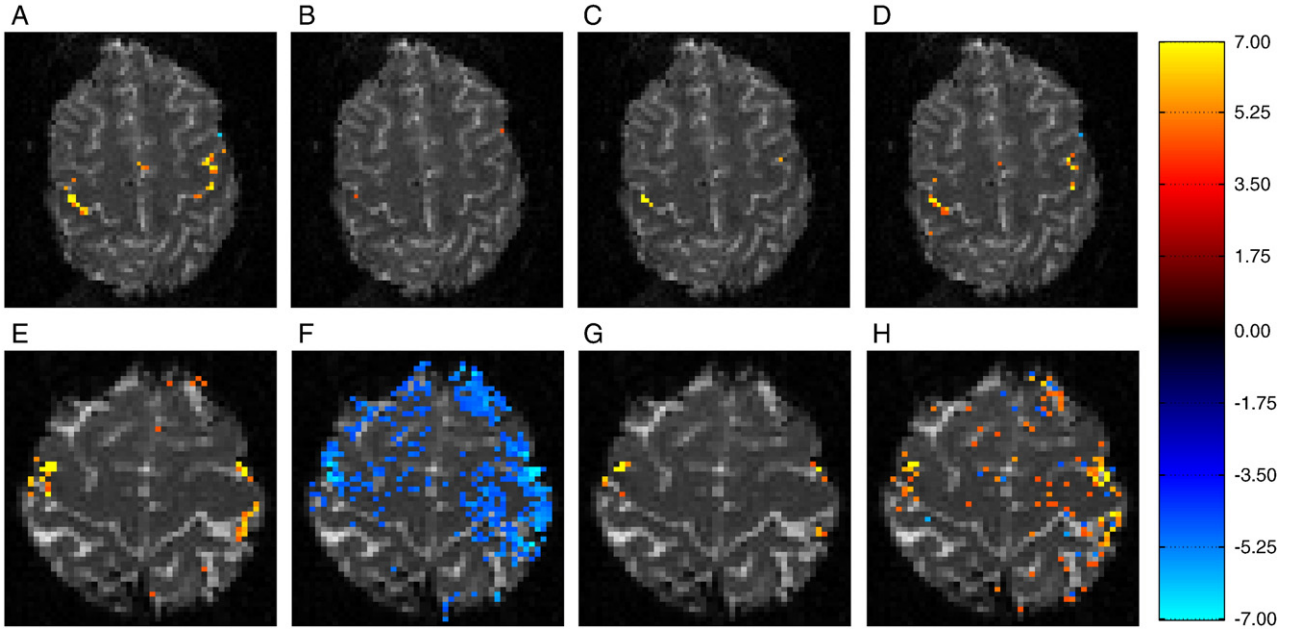

Fig. 5. Representative activations from the human data are shown in a parenchymal slice (first row) and venous slice (second row) cropped to the region around the brain. MO activations are shown in panels A and E, PO activations in panels B and F, CP activations in panels C and G, and PR activations in panels D and H. The CP activations are generally a subset of the MO activations, while the PR activations include many voxels which are not MO active. The PO time series suffers from several confounding factors and leads yield diffuse activations in panel F.

activations are seen in Fig. 5(F), as likely the result of task-related, out of field of view motion.

The parenchymal slice constant phase activations in Fig. 5(C) are a subset of the activations found through the magnitude-only method in Fig. 5(A). The constant phase activations in the parenchymal slice are a small subset of the magnitude-only activations, although the voxels do not exhibit statistically significant TPRCs. The reduction of constant phase activations is only partially explained by sub-threshold TRPCs. At this time, the data is not of sufficient quality to produce the stable phase time series required for the complex constant phase statistical model. The constant phase model is vulnerable to instabilities in the phase time series, not only phase instabilities which correlate with the task. In the real data, phase instabilities which are off the task frequency exist. Thus, in the parenchymal slice, both sub-threshold TRPCs and other temporal phase instabilities lead to lowering the statistical significance of the suspected constant phase parenchymal activations. As discussed later, modified acquisition techniques may improve the phase stability of the time series and thus improve the results of the constant phase model.

The results of the constant phase method in the venous slice (Fig. 5(G)) are also a small subset of the magnitude-only activations (Fig. 5(E)). As apparent in Fig. 5(F), significant TRPCs are observed in the MO active voxels with large TRPCs in the suspected draining veins. The constant phase method thus biases against the voxels with TRPCs as shown in the simulation. Voxels with large TRPCs coupled with large CNRs are found to be active while voxels with smaller CNRs are eliminated. This bias is likely the result of the observed TRPCs from the draining veins and, as in the parenchymal case, other unmodeled temporal phase variation.

The phase regressor activations in the parenchymal slice are shown in Fig. 5(D). These activations correlate quite well with the magnitude-only activations in the parenchymal slice. This is consistent with an ideal method designed to reduce draining vein contributions as the parenchymal slice activations are not eliminated. The statistical significance of the parenchymal slice activations is generally lower than found with the magnitude-only method, likely because of the sub-threshold TRPCs observed in these voxels. Thus, with sub-threshold TRPCs, the phase regressor activations in real parenchymal data are consistent with the simulated activations.

Venous slice activations found with the phase regressor method are shown in Fig. 5(H). These activations include several unexpectedly located activations which are not present in the magnitude-only or complex constant phase activations. These several unexpectedly located phase regressor activations throughout the brain result from errors in the regression of the magnitude as a function of phase when significant TRPCs are present. This is also seen in the simulation in Fig. 3(F) where the phase regressor method overcompensates for the positive correlation with task in the phase data in several voxels to yield unexpected positive phase regressor activations. In this experimental data, many voxels with negatively correlated task-related phase changes are found to have positive phase regressor activations as the simulation predicts. Thus, the confounding factors in the phase data which lead to unexpectedly located phase-only activations propagate into the phase regressor activations. This is clearly not a property which an ideal method for eliminating draining vein activations would exhibit.

The trends illustrated in the above representative data set extend through all subjects as shown in Table 1 which consolidates the data from all subjects. It is apparent that most of the constant phase activations are also magnitude-only activations. Fewer of the phase regressor activations are also magnitude-only activations as the problem of false positives arising from the problematic fit of magnitude as a function of phase. As both methods are argued to reduce magnitude-only activations by biasing against voxels with task-related phase changes, the constant phase method favorably finds a subset of the magnitude-only activations to be above threshold, while the phase regressor method appears to have an increased rate of false positives.

Table 1
Percentage of constant phase and phase regressor activations which are also magnitude only and phase only activations

	% Voxels also MO-active			% Voxels also PO-active		
	All slices	Parenchymal slices	Venous slices	All slices	Parenchymal slices	Venous slices
CP	85.6	86.8	88.8	15.7	14.8	20.4
PR	31.7	36.8	37.8	42.6	34.3	40.1

Further illustrating the problem of the phase regressor statistical method failing when significant TRPCs are present, the median phase-only activation statistic for the phase regressor active voxels is 4.62. This is significant with a relatively strong Bonferroni-adjusted $\alpha = 0.10$ threshold. The complex constant phase statistical model, which consistently exhibits a bias against voxels with large TRPCs in both the simulated and real data, however, has a median phase-only activation statistic of 1.95 in its active voxels. This is not significant with a weak, uncorrected $\alpha = 0.05$ threshold. Based only upon this, the complex constant phase statistical method appears more favorable.

However, the complex constant phase method is relatively conservative and finds a small subset of the magnitude-only activations to be active. Only 18.1% of the magnitude-only activations in all slices are also constant phase activations (14.5% in parenchymal slices and 22.7% in venous slices). In all cases, significant non-task-related phase changes in the real data challenge the complex constant phase model's assumption of constant phase, leading to reduced activation statistics. Only when large CNRs are present does the complex constant phase method find activations. Such CNRs are present in highly active cortex and de-localized veins with large TRPCs. As shown in the simulation, voxels with large TRPCs and large CNRs are not eliminated by the complex constant phase statistical method. It is the coupling of large TRPCs with large CNRs that leads to the increase of correspondence between the magnitude-only and complex constant phase activations in the venous slices.

The phase regressor method finds a higher percentage of the magnitude-only activations. In all slices, 56.1% of the magnitude-only activations are also phase regressor activations. In parenchymal slices, 59.9% of the magnitude-only activations are found, while 55.7% of the venous slice magnitude-only activations are active through the phase regressor method. This, of course, is tempered by the tremendous number of phase regressor activations which are not also magnitude-only activations.

Discussion and conclusion

The data presented in this manuscript raises challenges to the applicability of statistical activation methods which reduce draining vein contributions to real data. Simulations have revealed the vulnerability of the phase regressor statistical method to slight

errors in the estimates of the baseline magnitude and phase variance in the regression of magnitude as a function of phase. This leads to overcorrection of the magnitude data when large task-related phase changes are present in the data. This problem was illustrated in both simulated and real data with the presence of apparent false positives.

A current challenge of the complex constant phase method was also illustrated in the presented experimental data. As the method relies upon a reduced fit of the data to the constant phase model to eliminate draining vein activations, the complex constant phase statistical method also biases against voxels with non-task-related phase instabilities in current real data and unshown simulations. This problem was illustrated in the real data in this manuscript with the reduction of activations in parenchymal data with sub-threshold task-related phase changes.

Modifications to the implementations or data collection methods for both the phase regressor statistical method and the complex constant phase statistical method might need to be made for either to reliably bias only against voxels with task-related phase changes. Because the variance in the magnitude data is generally expected to be far greater than the variance in the phase data, an implementation of the phase regressor method assuming error only in the magnitude values is reasonable. Such unpublished implementations exist and preliminary investigations show that they reduce the false positives observed in this study. Further work needs to be done to evaluate different methods for computing the regression of magnitude as a function of phase in an attempt to reduce the vulnerability to overcorrections.

The complex constant phase statistical method relies upon data with a relatively temporally constant phase, and further work needs to be done to ensure the temporal stability of the global phase signal. This includes either filtering the acquired phase signal to remove non-task-related temporal variations, or collecting data with more temporally stable phase time series. The latter includes the acquisition of dynamic B-field maps with each TR to correct for global phase changes (Roopchansingh et al., 2003), the acquisition of smaller voxels where less dephasing can occur, and the reduction of TE to reduce the time for disparate phases to accrue. Furthermore, a complex data model which directly models both the magnitude and phase, with a phase reference function accounting for global B-field changes, such as that presented by Rowe (2005b), may yield improved results without the limitations of the constant phase restriction.

Once these models and data acquisition methods are improved to reliably bias against draining veins in simple quadrature-detected data, they could be generalized for use with multi-coil methods which are growing in popularity. Such receive coils can yield different phases for the same spatial locations in the reconstructed images from each channel. These different phases from each of the channels will clearly lead to complications in these statistical methods which utilize phase. Appropriate consideration for the phase in such multi-channel acquisitions should be examined so that these methods may be expanded to accommodate such data sets.

Acknowledgments

This work was supported in part by NIH T32MH019992, R01E00215 and R01AG020279. We would also like to thank the reviewers for their insightful suggestions.

Appendix A. Menon's complex phase regressor (PR) method

Unlike the traditional magnitude-only method, a two step method developed by Menon (2002) utilizes phase information in an attempt to bias against magnitude activations in voxels with associated task-related phase changes. Using the same standard Fourier reconstruction method, complex-valued images are formed and are converted into unique pairs of magnitude and phase images with the following standard transformations for magnitude and phase:

$$m_t = \sqrt{r_t^2 + i_t^2}. \tag{A.1}$$

$$\phi_t = \arctan\left(\frac{i_t}{r_t}\right). \tag{A.2}$$

In these equations, m_t is the calculated magnitude of the tth time point of a voxel time series, ϕ_t is the calculated phase of the tth time point, and r_t and i_t are the reconstructed real and imaginary observations at the tth time point, respectively. The phase and magnitude time series for each voxel are then considered. To reduce task-related changes in the magnitude in voxels with task-related phase changes, a least squares linear regression of magnitude values as a function of phase is computed for each voxel to create an estimated magnitude image:

$$m_{\text{est}} = \hat{B} + \hat{A}\phi \tag{A.3}$$

$$\hat{A} = \frac{-\left(S_{\phi\phi} - \frac{\hat{\sigma}_\phi^2}{\hat{\sigma}_m^2} S_{mm}\right) + \sqrt{-\left(S_{\phi\phi} - \frac{\hat{\sigma}_\phi^2}{\hat{\sigma}_m^2} S_{mm}\right)^2 + 4\frac{\hat{\sigma}_\phi^2}{\hat{\sigma}_m^2} S_{\phi m}^2}}{2\frac{\hat{\sigma}_\phi^2}{\hat{\sigma}_m^2} S_{\phi m}} \tag{A.4}$$

$$\hat{B} = \bar{m} - \hat{A}\,\bar{\phi} \tag{A.5}$$

where $\bar{m}$ is the arithmetic mean of the magnitude time series, and $\bar{\phi}$, $S_{\phi\phi}$, S_{mm}, and $S_{\phi m}$ are defined to be:

$$\bar{\phi} = \arctan\left(\frac{\frac{1}{n}\sum_{t=1}^{n} \sin\phi_t}{\frac{1}{n}\sum_{t=1}^{n} \cos\phi_t}\right) \tag{A.6}$$

$$\Delta\phi = \arctan\left(\frac{\Im\left(\frac{r_t + i_t}{\bar{m}\ \exp i^*\phi}\right)}{\Re\left(\frac{r_t + i_t}{\bar{m}\ \exp i^*\phi}\right)}\right) \tag{A.7}$$

$$S_{\phi\phi} = \sum_{t=1}^{n} (\Delta\phi)^2 \tag{A.8}$$

$$S_{mm} = \sum_{t=1}^{n} (m_t - \bar{m})^2 \tag{A.9}$$

$$S_{\phi m} = \sum_{t=1}^{n} (\Delta\phi)(m_t - \bar{m}). \tag{A.10}$$

In these formulae, $\hat{B}$ and $\hat{A}$ are determined through a least squares regression with normally distributed errors in both m and ϕ (Casella and Berger, 1990). The $\Re$ and $\Im$ symbols indicate taking the real and imaginary components of the complex-valued element. The estimated variances, $\hat{\sigma}_{\phi}^2$ and $\hat{\sigma}_{m}^2$, are determined individually for each voxel by taking the FT of the time series, setting the task frequency and its first four harmonics to zero, and then calculating the variance of the filtered time series after taking the IFT (Menon, 2002). Because the phase time series can wrap around, circular statistics were implemented to determine the average phase, ϕ, and difference in phase, $\Delta\phi$, without the need to unwrap the phase time series (Jammalamadaka and SenGupta, 2001). Using the phase image time series, estimated magnitude image time series are created using the above described linear regression. The phase-estimated magnitude ($m_{\phi t}=\hat{A}_{\phi t}$) is then subtracted from the observed magnitude, ideally leaving corrected magnitude time series with no magnitude changes in voxels with TRPCs. The same general linear model used in the magnitude activation method is then used to compute cortical activations for the corrected magnitude time series. This model was introduced with an empirical linear fit of the phase's effect on magnitude observations. However, it is not clear that a linear fit is optimal, as some data suggests a more complicated relationship (Klassen and Menon, 2005).

Appendix B. Rowe and Logan's complex constant phase (CP) method

The Rowe–Logan complex constant phase method (Rowe and Logan, 2004) is different from the previous method in that it directly utilizes the information in the complex-valued reconstructed images to compute magnitude activations. This both avoids the large signal-to-noise ratio assumption of normally distributed noise for the Ricean noise in the magnitude-only images, and utilizes twice as many data points to compute the maximum likelihood estimators, leading to a theoretically improved power of determining true activations (Rowe, 2005c). The model for data in this case is:

$$\begin{pmatrix} R \\ I \end{pmatrix} = \begin{pmatrix} X & 0 \\ 0 & X \end{pmatrix} \begin{pmatrix} \beta\cos\theta \\ \beta\cos\theta \end{pmatrix} + \eta, \qquad \eta \sim N\left(0,\, \sigma^2 I_{2n}\right). \tag{B.1}$$

In this equation, the left-hand side is the vector of observed real data ($R=(r_1, \ldots, r_n)'$) stacked on top of the vector of imaginary data ($I=(i_1, \ldots, i_n)'$); X is the same design matrix as in the magnitude-only activation method; β is the same vector of regression coefficients as in the magnitude-only activation method; and θ is the fixed but unknown phase angle of the data which is estimated on a voxel-wise basis. As with the other methods, hypothesis tests which consider the value of β_2 are used to determine the activation statistics for each voxel. In this activation method, the phase angle θ is assumed to be temporally constant, and is thus represented by its maximum likelihood estimator in both the unrestricted alternative hypothesis and in the restricted null hypothesis. The maximum likelihood estimators for the unrestricted case, $\beta_2 \neq 0$, can be shown to be:

$$\hat{\beta} = \hat{\beta}_R \cos\hat{\theta} + \hat{\beta}_I \sin\hat{\theta} \tag{B.2}$$

$$\hat{\sigma}^2 = \frac{1}{2n}\left[\begin{pmatrix} R \\ I \end{pmatrix} - \begin{pmatrix} X\hat{\beta}\cos\hat{\theta} \\ X\hat{\beta}\sin\hat{\theta} \end{pmatrix}\right]' \left[\begin{pmatrix} R \\ I \end{pmatrix} - \begin{pmatrix} X\hat{\beta}\cos\hat{\theta} \\ X\hat{\beta}\sin\hat{\theta} \end{pmatrix}\right] \tag{B.3}$$

$$\hat{\theta} = \frac{1}{2}\arctan\left[\frac{\hat{\beta}_I'(X'X)\hat{\beta}_R}{\left(\hat{\beta}_R'(X'X)\hat{\beta}_R - \hat{\beta}_I'(X'X)\hat{\beta}_I\right)/2}\right] \tag{B.4}$$

$$\hat{\beta}_R = (X'X)^{-1}X_R'R \tag{B.5}$$

$$\hat{\beta}_I = (X'X)^{-1}X_I'I. \tag{B.6}$$

The maximum likelihood estimators for the null hypothesis, $\beta_2=0$, or more generally $C\beta=0$ with $C=(0, 0, 1)$ in this case, can be shown to be:

$$\tilde{\beta} = \Psi\left[\hat{\beta}_R\cos\tilde{\theta} + \hat{\beta}_I\sin\tilde{\theta}\right] + (X'X)^{-1}C'\left[C(X'X)^{-1}C'\right]^{-1} \tag{B.7}$$

$$\tilde{\sigma}^2 = \frac{1}{2n}\left[\begin{pmatrix} R \\ I \end{pmatrix} - \begin{pmatrix} X\tilde{\beta}\cos\tilde{\theta} \\ X\tilde{\beta}\sin\tilde{\theta} \end{pmatrix}\right]' \left[\begin{pmatrix} R \\ I \end{pmatrix} - \begin{pmatrix} X\tilde{\beta}\cos\tilde{\theta} \\ X\tilde{\beta}\sin\tilde{\theta} \end{pmatrix}\right] \tag{B.8}$$

$$\tilde{\theta} = \frac{1}{2}\arctan\left[\frac{\hat{\beta}_R'\Psi(X'X)\tilde{\beta}_I}{\left(\hat{\beta}_R'\Psi(X'X)\hat{\beta}_R - \hat{\beta}_I'\Psi(X'X)\hat{\beta}I\right)/2}\right]. \tag{B.9}$$

In these equations, Ψ is the same as in the magnitude-only method. As with the magnitude-only method, these maximum likelihood estimators can be used to test for significance of β_2 utilizing a likelihood ratio statistic with a large sample χ^2 distribution under the null hypothesis, where d is once again the full row rank of C or the degrees of freedom:

$$-2\log\lambda_{\mathrm{CP}} = n\log\frac{\hat{\sigma}^2}{\tilde{\sigma}^2}. \tag{B.10}$$

In this case, the χ^2 statistics can be manipulated to approach F or t statistics asymptotically for large samples. In this paper, large sample z-statistics are considered through the transformation of:

$$Z_{\mathrm{CP}} = \mathrm{sign}(C\hat{\beta})\sqrt{-2\log(\lambda_{\mathrm{CP}})} \tag{B.11}$$

The activation statistics can then be thresholded to determine activations.

This complex constant phase method has also been argued to remove voxels declared active as the result of TRPCs associated with draining veins (Nencka and Rowe, 2005; Rowe and Nencka, 2006). While not explicitly relying upon a mathematical model of the phase behavior, this method assumes that θ is fixed to be temporally constant but unknown in each voxel, while varying from voxel-to-voxel. By assuming that the angle θ is represented by its maximum likelihood estimator for the voxel time series, a constant phase condition is assumed in the individual voxel time series. When this condition is not met as a voxel exhibits task-related phase changes, the assumptions of the model are not satisfied, making the fit constant phase suboptimal. This results in larger residual variances in the model, $\hat{\sigma}^2$, and thus lower activation statistics. It is this reduced fit, not the explicit modeling of the phase response, that has been claimed to reduce draining vein contributions. Therefore, the complex constant phase activa-

tion method theoretically biases against declaring such voxels active. It should be noted that allowing the angle θ to be estimated at each time point has been shown to remove any phase dependence in the model, yielding the magnitude-only activation method (Rowe and Logan, 2005). Further, in a more general activation method the phase angle θ_t has been modeled in a linear fashion along with the magnitude (Rowe, 2005b).

References

Bandettini, P.A., Jesmanowicz, A., Wong, E.C., Hyde, J.S., 1993. Processing strategies for time-course data sets in functional MRI of the human brain. Magn. Reson. Med. 30, 161–173.

Casella, G., Berger, R.L., 1990. Statistical Inference. Wadsworth and Brooks/Cole, Pacific Grove, CA.

Cox, R.W., Jesmanowicz, A., Hyde, J.S., 1995. Real-time functional magnetic resonance imaging. Magn. Reson. Med. 33, 230–236.

Gonzalez, R.C., Woods, R.E., 1992. Digital Image Processing. Addison-Wesley Publishing Company, Reading, MA, USA.

Haacke, E.M., Brown, R., Thompson, M., Venkatesan, R., 1999. Magnetic Resonance Imaging: Physical Principles and Sequence Design. John Wiley and Sons, New York, NY, USA.

Jammalamadaka, S., SenGupta, A., 2001. Topics in Circular Statistics. World Scientific, Singapore.

Klassen, L., Menon, R., 2005. BOLD signal phase and magnitude dependence on vessel geometry. Proc. Int. Soc. Magn. Reson. Med. 13, 496.

Lai, S., Glover, G.H., 1997. Detection of BOLD fMRI signals using complex data. Proc. Soc. Magn. Reson. Med. 3, 1671.

Logan, B.R., Rowe, D.B., 2004. An evaluation of thresholding techniques in fMRI analysis. NeuroImage 22, 95–108.

Menon, R.S., 2002. Postacquisition suppression of large-vessel BOLD signals in high-resolution fMRI. Magn. Reson. Med. 47, 1–9.

Nan, F.Y., Nowak, R.D., 1999. Generalized likelihood ratio detection for fMRI using complex data. IEEE Trans. Med. Imag. 18, 320–329.

Nencka, A.S., Rowe, D.B., 2005. Complex constant phase method removes venous BOLD component in fMRI. Proc. Int. Soc. Magn. Reson. Med. 13, 495.

Nencka, A.S., Rowe, D.B., 2006. Theoretical results demonstrate fundamental differences in venous BOLD reducing fMRI activation methods. Proc. Int. Soc. Magn. Reson. Med. 14, 3269.

Ogawa, S., Menon, R.S., Tank, D.W., Kim, S.G., Merkle, H., Ellermann, J.M., Ugurbil, K., 1993. Functional brain mapping by blood oxygen level-dependent contrast magnetic resonance imaging. Biophys. J. 64, 803–812.

Pfeuffer, J., Van de Moortele, P.F., Ugurbil, K., Hu, X., Glover, G.H., 2002. Correction of physiologically induced global off-resonance effects in dynamic echo-planar and spiral functional imaging. Magn. Reson. Med. 47, 344–353.

Roopchansingh, V., Cox, R.W., Jesmanowicz, A., Ward, B.D., Hyde, J.S., 2003. Single-shot magnetic field mapping embedded in echo planar time-course imaging. Magn. Reson. Med. 50, 839–843.

Rowe, D.B., 2005a. Complex activation is more focal and concentrated to parenchymal tissue. Proc. Int. Soc. Magn. Reson. Med. 13, 1575.

Rowe, D.B., 2005b. Modeling both the magnitude and phase of complex-valued fMRI data. NeuroImage (25), 1310–1324.

Rowe, D.B., 2005c. Parameter estimation in the magnitude-only and complex-valued fMRI data models. NeuroImage (25), 1124–1132.

Rowe, D.B., Logan, B.R., 2004. A complex way to compute fMRI activation. NeuroImage 23, 1078–1092.

Rowe, D.B., Logan, B.R., 2005. Complex fMRI analysis with unrestricted phase is equivalent to a magnitude-only model. NeuroImage 24, 603–606.

Rowe, D.B., Nencka, A.S., 2006. Complex activation surpresses venous BOLD in GE–EPI fMRI data. Proc. Int. Soc. Magn. Reson. Med. 14, 2834.

Rowe, D.B., Meller, C.P., Hoffmann, R.G., 2007a. Characterizing phase-only fMRI data with an angular regression model. J. Neurosci. Methods 161, 331–341.

Rowe, D.B., Nencka, A.S., Hoffmann, R.G., 2007b. Signal and noise of Fourier reconstructed fMRI data. J. Neurosci. Methods 159, 361–369.

Smith, A.M., Lewis, B.K., Ruttimann, U.E., Ye, F.Q., Sinnwell, T.M., Yang, Y., Duyn, J.H., Frank, J.A., 1999. Investigation of low frequency drift in fMRI investigation. NeuroImage (9), 526–533.

Turner, R., 2002. How much cortex can a vein drain? Downstream dilution of activation-related cerebral blood oxygenation changes. NeuroImage 16, 1062–1067.